Original Article
DOI: https://doi.org/10.70749/ijbr.v3i6.1724

INDUS JOURNAL OF BIOSCIENCE RESEARCH
https://induspublishers.com/IJBR
ISSN: 2960-2793/ 2960-2807

Computer-Aided Analysis of Oxino-*bis*-Pyrazolederivative as a Potential Breast Cancer Drug Based on DFT, Molecular Docking, and Pharmacokinetic Studies: Compared with the Standard Drug Tamoxifen

Muhammad Amir Abbas[1], Muhammad Zahid Khan[2], Hafiz Muhammad Atif[3], Asim Shahzad[3], Jamaluddin Mahar[4]

[1]Institute of Chemistry, The Islamia University of Bahawalpur, Punjab, Pakistan.
[2]Department of Peads, Nishtar Medical University, Multan, Punjab, Pakistan.
[3]Department of Urology and Kidney Transplant, Benazir Bhutto Hospital, Rawalpindi, Punjab, Pakistan.
[4]Department of Chemistry, Qaid-E-Azam University, Islamabad, Pakistan.

ARTICLE INFO

Keywords: Oxino-bis-Pyrazole derivative, Breast cancer, DFT analysis, Molecular docking, Pharmacokinetics.
Correspondence to: Muhammad Amir Abbas
Institute of Chemistry, The Islamia University Bahawalpur, Punjab, Pakistan.
Email: muhammadamirabbas@gmail.com

Declaration

Authors' Contribution

MAA wrote the main manuscript Draft, writing, computational work, **JM** supervision, **AS** studied Data validation and **HMA & MZK** Editing, Reviewing. All authors reviewed the manuscript outline

Conflict of Interest: No conflict of interest.

Funding: No funding received by the authors.

Article History

Received: 12-03-2025 Revised: 10-06-2025
Accepted: 23-06-2025 Published: 30-06-2025

ABSTRACT

Breast cancer is the most often diagnosed and deadliest type of cancer in the world. Thiophene derivatives are available with various biological and pharmacological properties. In the current study, Computer assisted toxicity and pharmacokinetics prediction has been considered by pharmaceutical industries as an efficient way of choosing the potential drug. This study aimed at evaluating the in-silico pharmacokinetic properties (ADME) and toxicity and drug likeness of eight drugs. This work applies SwissADME, Pro Tox II, molinspirastion, and ADMETlab web applications and a quantum chemical investigation using density function theory (DFT) was utilized to explore the structural characteristics of thiophene derivatives, and the breast cancer inhibitory properties were revealed through molecular docking simulation. The optimization of the lead molecule was initially performed using DFT/B3LYP approach with a 6-31++(d,p) base set. The simulated electrostatic potential was performed to evaluate the reactivity of the lead molecule, and the molecular reactivity and stability were evaluated through HOMO-LUMO analysis based on energy gap, chemical potential (μ), electronegativity (χ), hardness (η), and softness (S) values. Then molecular docking research was used to assess the interaction of thiophene derivatives against the breast cancer target proteins, and pharmacokinetic evaluation was used to evaluate the drug-likeness property of the lead molecule. The leading molecules showed no violation against Lipinski's rule, and the highest binding affinity was observed against HER-2 (PDB ID: 2IOK) with a docking score of -9.45Kcal/mol.

Graphical Abstract

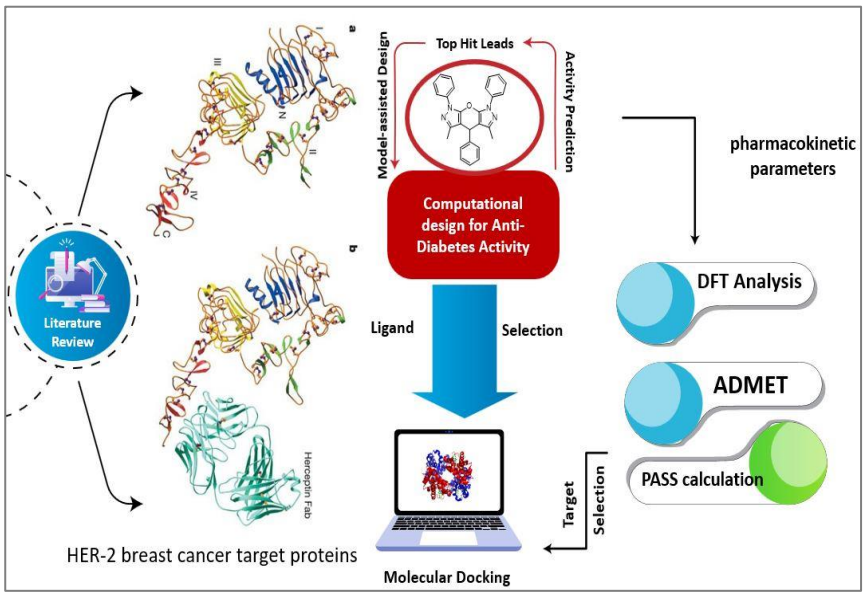

INTRODUCTION

Computational pharmacology is a rapidly expanding scientific discipline directed toward advances in technologies for using computer software and databases to construct and analyze molecular, biological, and medication information from various sources [1, 2]. The methods have been in use since the beginning of a drug discovery process in order to screen and identify new lead compounds available in molecular libraries [3–5], and in doing so achieving parallel optimization of compound efficiency, drug-like properties, and thus contributing to the improvement of the quality of a drug candidates. The design and development of drug molecules involve consideration of pharmacokinetic properties, main analysis of absorption, distribution, metabolism and excretion (ADME) at a stage when there are multiple compounds under consideration, but with restricted physical specimen [3, 7]. Because of formidable barriers in pharmacokinetic and toxicity profiles of new drug like molecules, only one in ten drug candidates make it to the clinical development stage to hit the market [4, 8]. In the end,the pharma industries still stay under pressure to reverse the high rate of drop out in drug production that lead to the increased interest in computer aided toxicity and pharmacokinetic profile prediction [9]. Computer aided approaches provide tremendous opportunities for the effective identification of new drug-like molecules using less time and costs compared to the experimental approaches [10, 11]. Consequently, there has been marvelous advancement in the field of computer aided drug designing and computational chemistry. These methods have been applied in screening of new chemical species and their chemical properties cha.[12] On the hand, there is web-based tools namely ADMETlab, Pro Tox-II and SwissADME which have been designed to predict ADMET properties [3, 4, 13].

Breast cancer is common in women across the world In Pakistan according to ICMR new breast cancer cases were 1, 40, 000 and the age group affected was 20-60 years [Louhi-Kultanen et al., 2003]. Therefore, the treatment of breast cancer is through chemotherapy that inclines in the function of receptors. The estrogen receptor (ER) presents the activity of breast cancer initiation and progression, although the progesterone receptor (PR) was typically over expressed in breast cancer [13,14]. The overexpression of progesterone receptor and estrogen receptor brings a prognosis of breast cancer growth and shows good possibility of response to hormonal treatment [15]. In triple negative breast cancer (TNBC), egfr is major, and the alternate treatment option for TNBC was very limited since they are phenotypically different as PR negative, ER negative, and HER 2 negative[16]. Hence the targeting of epidermal growth factor receptors is a good treatment approach. , for those proteins viewed as target proteins, it can be argued that the chemokine ligand 18 (CCL18) could be seen as a target protein in breast cancer as the chemokine was derived from tumor associated macrophages (TAMs) to suitable breast cancer metastasis [17]. B-cell lymphoma 2 (BCL2) is a group of a protein family involved in anti-apoptotic protein mentioned in the inner mitochondria membrane signaling [18]. The metastatic pathway in breast cancer was implicated by cell cycle regulators, transcriptional factors and tyrosine kinase. They bind and suppress HSP90, illustrating its good therapeutic effect on breast cancer [19]. A promising target for novel human breast cancer therapy was glycogen synthase kinase-3 (GSK-3). Its inhibition decreases the survival of breast cancer cells [20], and mutation in the gene that undergoes tumor suppressor PTEN gene deleted on 10th chromosome causes non-control of the PI3K pathway. Of these downstream effectors of PI3Ks, PDK1 (3- phosphoinositide-dependent protein kinase 1) has a major function in cancers [21]. PAK4 in BC For a little more interest PAK4 is overexpressed in Primary Human Breast Cancer and Breast Cancer Cell Lines and rat tumor samples. Nonetheless, it was only faintly detectable in normal tissues [22]. Therefore, these different kinds of breast cancer proteins may be possibly used as drug targets to treat breast cancer. In this current study DFT was performed for thiophene derivatives to describe the more stable molecular geometry, reactivity, charge transfer stabilization interactions and probable reactive sites [23] Molecular docking simulations have been also carried out to describe the interactions of ligand with the target protein and also the potential energy of binding of protein-ligand interaction [24] ADMET evaluation has been also done to describe the safety profile of the lead molecule. Due to these reasons, Biochanin A was analysed for the combined effects of DFT quantum chemical investigation and Molecular docking simulation which would be useful for both in-vitro and in-vivo tests. The DFTstudy was carried out using the Gaussian 09W program package and the molecular docking simulation using Maestro software. The current study offers a distillate computation of the lead molecule in combating breast cancer, and can be insightful for drug development under in-vitro and in-vivo distress.

Design of Novel Drug Compounds (KJ. 1-4)

On the basis of our understanding of the available literature no theoretical works have been reported on Oxino-bis-Pyrazole derivative till now. This is the first systematic investigation of these novel and highly elongated Pyrazole derivatives. What can be found on paper includes sections involving computational information such as frontier molecular orbitals, the electro-optical aspect, pharmacokinetics and the results involving docking.In the context of drug discovery and development, the three-dimensional crystal structure of Pyrazole-based compounds as well as the canonical SMILES notation of the molecules are clearly of critical importance. These compounds can be easily studied with regards to drug like property using ADMET analysis or molecular docking studies. These give one and opportunity of making ADMET evaluation on the OBP derivatives. (SMILES: CC1=NN(C2=CC=CC=C2)C3=C1C(C4=CC=CC=C4)C5=C(O3)N(C6=CC=CC=C6)N=C5C).

Table 1

2D, 3D structures and SMILES of the selected ligands from KJ-1 to KJ-4

codes	Ligands	2D structure	3D structure	SMILES
KJ 1	3,5-dimethyl-1,4,7-triphenyl-4,7-dihydro-1H-pyrano[2,3-c:6,5-c'] dipyrazole	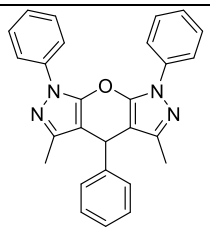	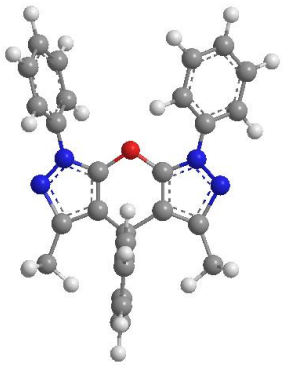	CC1=NN(C2=CC=CC=C2)C3=C1C(C4=CC=CC=C4)C5=C(O3)N(C6=CC=CC=C6)N=C5C
KJ 2	4-(4-bromophenyl)-3,5-dimethyl-1,7-diphenyl-4,7-dihydro-1H-pyrano[2,3-c:6,5-c'] dipyrazole	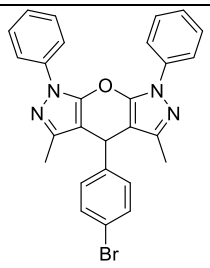	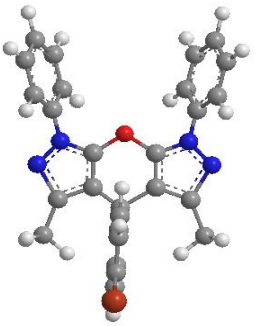	CC1=NN(C2=CC=CC=C2)C3=C1C(C4=CC=C(Br)C=C4)C5=C(O3)N(C6=CC=CC=C6)N=C5C
KJ 3	4-(3,5-dimethyl-1,7-diphenyl-4,7-dihydro-1H-pyrano[2,3-c:6,5-c'] dipyrazol-4-yl)phenol	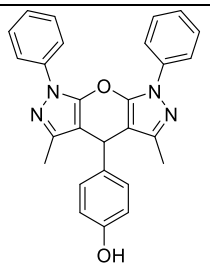	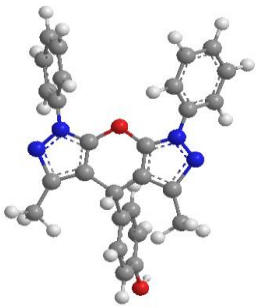	OC1=CC=C(C(C2=C3N(C4=CC=CC=C4)N=C2C)C5=C(O3)N(C6=CC=CC=C6)N=C5C)C=C1
KJ 4	4-(benzo[d][1,3]dioxol-5-yl)-3,5-dimethyl-1,7-diphenyl-4,7-dihydro-1H-pyrano[2,3-c:6,5-c']dipyrazole	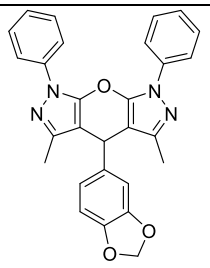	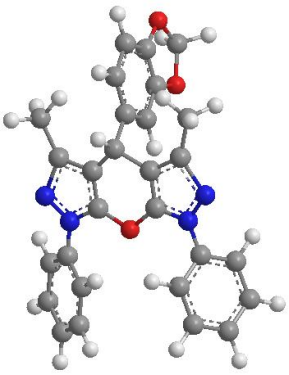	CC1=NN(C2=CC=CC=C2)C3=C1C(C4=CC=C(OCO5)C5=C4)C6=C(O3)N(C7=CC=CC=C7)N=C6C
Drug I	2-{2-[4-({5-chloro-6-[3-(trifluoromethyl)phenoxy]pyridin-3-yl}amino)-5H-pyrrolo[3,2-d]pyrimidin-5-yl]ethoxy}ethanol	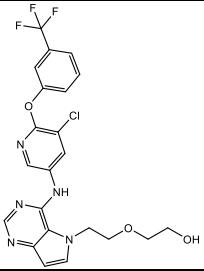	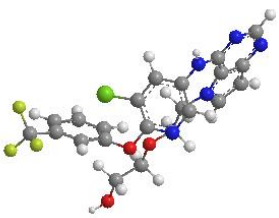	OCCOCCN(C=CC1=NC=N2)C1=C2NC3=CC(Cl)=C(N=C3)OC4=CC=CC(C(F)(F)F)=C4

Drug II	Tamoxifen	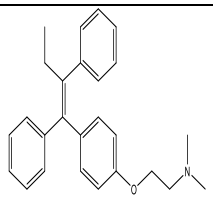	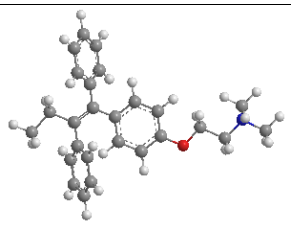	CN(CCOC1=CC=C(/C(C2=CC=CC=C2)=C(CC)\C3=CC=CC=C3)C=C1)C

DFT and Related Information

The complete molecular structure optimization of the observed compound was performed by Gaussian 16 desktop software and Density Functional Theory B3LYP/6-31++G (d, p) basis set. The authors used the Gaussian software package for the DFT optimization geometry of the examined compounds (Tegegn, D. F., 2024). In the optimization process the B3LYP theory level with 6-31G(d,p) basis sets were used. The optimized structures were further employed to calculate that energy of highest occupied molecular orbital (HOMO) and the energy of the lowest unoccupied molecular orbital (LUMO). To assess the chemical reactivity of the target compounds, various chemical descriptor parameters were computed which include; energy gap (ΔE), ionization potential (IP), electron affinity (EA), electron delocalization (χ), electronic chemical potential (μ), chemical hardness (η), and softness (S). Before performing molecular docking, the initially optimized structure of the title molecule was generated and saved as one PDB format file using PyMol program (Elangovan, N., 2024). The selected proteins (PDB codes: (2IOK) was then downloaded in PDB format from an online tool and then docking done using autodock tools.

Optimized Geometry

The structure optimization and zero point energy of the compound in B3LYP/6-31++G(d,p) and Are -1336.395329, -3907.525870, -1411.621892 and -1524.930343Hartree,respectively. The bond length analysis across the four KJ derivatives (KJ 1–4) reveals consistent trends in key structural motifs, with aromatic C–C bonds (e.g., C5–C1, C9–C8) maintaining typical lengths of ~1.38 Å, indicative of delocalized π-systems, while C–N bonds (e.g., N10–C7, N18–C9) average ~1.36 Å, reflecting partial double-bond character. Notably, C–O bonds (e.g., O6–C7, O34–C6) are consistently shorter (~1.37–1.38 Å), underscoring their polar nature. Substituent-specific variations emerge, such as the Br33–C6 bond in KJ 2 (1.904 Å) being replaced by shorter O33–C6 bonds in KJ 3 (1.371 Å) and KJ 4 (1.378 Å), highlighting the influence of electronegative atoms. Terminal C–H bonds remain stable (~1.08–1.10 Å), while deviations in exocyclic bonds (e.g., C32–C2 in KJ 1 at 1.497 Å vs. C19–C15 in KJ 3–4) suggest conformational flexibility. Overall, the data demonstrate conserved core geometries with localized perturbations driven by substituent effects, aligning with trends observed in analogous heterocyclic systems. The CN bond distance C21–N18evaluated in the present work with DFT (B3LYP) methods are 1.421 Å for both the basis sets(Table 2).

Table 2

Optimized parameters of Pyrazole derivatives calculated by DFT (B3LYP)

KJ 1	Bond length (Å)	KJ 2	Bond length (Å)	KJ 3	Bond length (Å)	KJ 4	Bond length (Å)
C5C1	1.378	C9C8	1.378	C9C8	1.377	C6C5	1.396
C2C1	1.424	C7C8	1.515	C7C8	1.516	C1C6	1.379
C9C1	1.515	C12C7	1.515	C12C7	1.516	O34C6	1.378
C8C9	1.514	C11C12	1.378	C11C12	1.377	C4C5	1.379
C7C8	1.377	C15C12	1.425	C15C12	1.425	O33C5	1.378
C12C8	1.424	C16C8	1.425	C16C8	1.425	C2C1	1.411
O6C7	1.37	O10C9	1.369	O10C9	1.369	C3C4	1.413
N10C7	1.361	N18C9	1.36	N18C9	1.361	C7C3	1.534
N3C2	1.33	N13C11	1.36	N13C11	1.361	C8C7	1.516
C13C9	1.534	C3C7	1.532	C3C7	1.533	C12C7	1.516
C14C13	1.4	C2C3	1.398	C2C3	1.397	C9C8	1.377
C18C13	1.402	C4C3	1.401	C4C3	1.404	C11C12	1.377
C15C14	1.399	C1C2	1.398	C1C2	1.399	C15C12	1.425
C16C15	1.396	C5C4	1.394	C5C4	1.392	C16C8	1.425
C17C18	1.395	C6C1	1.392	C6C1	1.397	O10C9	1.369
C20N10	1.421	C21N18	1.422	C21N18	1.421	N18C9	1.361
N11N10	1.374	N17N18	1.374	N17N18	1.374	N13C11	1.361
C26C20	1.4	C22N13	1.422	C22N13	1.422	C21N18	1.421
C30C20	1.4	N14N13	1.374	N14N13	1.374	N17N18	1.374
C27C26	1.396	C23C21	1.401	C23C21	1.401	C22N13	1.422
C28C27	1.397	C27C21	1.401	C27C21	1.401	N14N13	1.374
C29C30	1.394	C24C23	1.397	C24C23	1.397	C23C21	1.401
N4C5	1.363	C25C24	1.397	C25C24	1.397	C27C21	1.401
C19N4	1.422	C26C27	1.394	C26C27	1.394	C24C23	1.397
C21C19	1.4	C28C22	1.401	C28C22	1.401	C25C24	1.397
C25C19	1.402	C32C22	1.401	C32C22	1.401	C26C27	1.394
C22C21	1.396	C29C28	1.394	C29C28	1.394	C28C22	1.401
C23C22	1.396	C30C29	1.398	C30C29	1.398	C32C22	1.401

C24C25	1.394	C31C32	1.397	C31C32	1.397	C29C28	1.394
C32C2	1.497	Br33C6	1.904	O33C6	1.371	C30C29	1.398
H34C14	1.088	H34C1	1.084	H34C1	1.088	C31C32	1.397
H35C15	1.086	H35C2	1.087	H35C2	1.088	C35O34	1.435
H36C16	1.086	H36C4	1.086	H36C4	1.087	H36C1	1.084
H37C17	1.086	H37C5	1.084	H37C5	1.085	H37C2	1.087
H38C18	1.087	H45C23	1.083	H45C23	1.083	H38C4	1.085
H39C21	1.082	H46C24	1.086	H46C24	1.086	H46C23	1.083
H40C22	1.086	H47C25	1.086	H47C25	1.086	H47C24	1.086
H41C23	1.086	H48C26	1.086	H48C26	1.086	H48C25	1.086
H42C24	1.086	H49C27	1.083	H49C27	1.083	H49C26	1.086
H43C25	1.083	H50C28	1.083	H50C28	1.083	H50C27	1.083
H44C26	1.083	H51C29	1.086	H51C29	1.086	H51C28	1.083
H45C27	1.086	H52C30	1.086	H52C30	1.086	H52C29	1.086
H46C28	1.086	H53C31	1.086	H53C31	1.086	H53C30	1.086
H47C29	1.086	H54C32	1.083	H54C32	1.083	H54C31	1.086
H48C30	1.083	C19C15	1.497	C19C15	1.497	H55C32	1.083
C31C12	1.497	C20C16	1.497	C20C16	1.497	C19C15	1.497
H33C9	1.1	H38C7	1.1	H38C7	1.101	C20C16	1.497
H49C31	1.096	H39C19	1.092	H39C19	1.092	H39C7	1.1
H50C31	1.095	H40C19	1.096	H40C19	1.096	H56C35	1.099
H51C31	1.092	H41C19	1.095	H41C19	1.095	H57C35	1.091
H52C32	1.092	H42C20	1.096	H42C20	1.096	H40C19	1.092
H53C32	1.095	H43C20	1.092	H43C20	1.092	H41C19	1.096
H54C32	1.096	H44C20	1.095	H44C20	1.095	H42C19	1.095
				H55O33	0.966	H43C20	1.096
						H44C20	1.092
						H45C20	1.095

Figure 1

Optimized geometry of titled compounds KJ 1, KJ 2, KJ 3 and KJ 4 using DFT/B3LYP methods with 6-31++G (d,p).

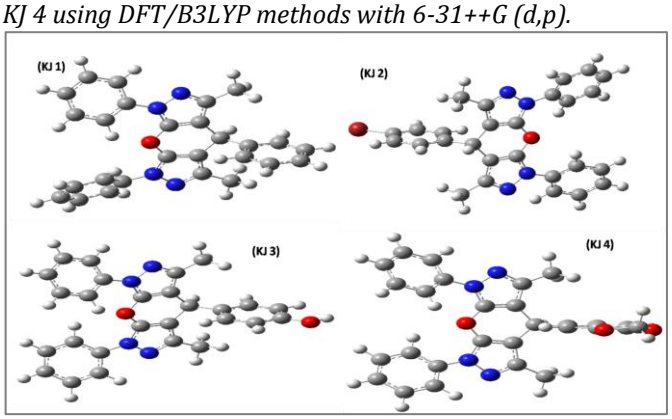

Quantum Molecular Descriptors and Electronic Properties

The electronic properties of the KJ series (KJ 1–4) reveal systematic variations in frontier molecular orbital energies, with KJ 2 exhibiting the deepest HOMO level (EH = –6.2588 eV) and highest ionization potential (IP = 6.2588 eV), suggesting superior oxidative stability. The energy gap (ΔE) narrows from KJ 1 (5.1285 eV) to KJ 4 (4.9353 eV), correlating with increased softness (S = 0.183 eV^{-1}) and reduced chemical hardness (η = 5.465 eV), indicative of enhanced polarizability and charge-transfer propensity in KJ 4. Notably, KJ 2's elevated electrophilicity index (ω = –0.658 eV) and electrochemical potential (μ = –3.726 eV) imply stronger electron-accepting character, while KJ 4's lower electronegativity (χ = 6.527 eV) and μ (–3.528 eV) suggest a more nucleophilic profile. These trends highlight a tunable electronic structure across the series, with KJ 2 optimized for stability and KJ 4 for reactivity, offering strategic insights for tailored material design. In order to analyze the electronic properties and nature of oxino-bis-pyrazole qualitatively, the FMO analysis is done. The energies of the HOMOs (E_{HS}), LUMOs (ELs) and energy gaps between the two (E_{H-L}) calculated for the isolated oxino-bis-pyrazole are tabulated in Table#3. The HOMO-LUMO energy gap (E_{H-L}) calculation for isolated (KJ1) is of about 5.13 eV. Following heterogroup decoration, the EH-L values drop from a high of 4.94 eV for KJ4 to a low of 4.40 eV for SCS. This is due to variations of EHOMO and ELUMO in all complexes of the nanomaterials under investigation. Comparing with KJ2, both KJ3 and KJ4 show an increase in EHOMO while a decrease in ELUMO, causing substantial decrease in EH-L. Next, the Ilien and Ouellet defined the EHOMO, ELUMO and EH-L for the KJ1 complex as -6.1622 eV, -1.033 eV and 5.1285 eV respectively. The complex was assigned with the E_{HOMO} of -6.2588 eV, E_{LUMO} of -1.1945 eV and E_{H-L} of 5.0642 eV. The largest gap is observed within the KJ1 complex. The EHOMO, ELUMO, and E_{H-L} for the KJ3 complex are found to be -6.1415 eV, -1.0601 eV, and 5.0815 eV, respectively. Discussing the idea of chromophores as the source of STABLE response, Fonseca et al. specified that complexes with the smaller HOMO LUMO gap may demonstrate superior characteristics (Mohapatra, R. K., et al2021).The maximum occupied molecular orbital (HOMO) energies, according to FMO research, vary from -6.1622 to -5.9964 eV (**Table 3**).Surplus electrons are not tightly bonded. Thus, excess electron behavior is seen in examined oxino-bis-pyrazole clusters, which may be a characteristic of importance for stability.

The energy gap calculation is as clearly illustrates in the following (see Fig. 2). Table 7 comprises of a number of molecular descriptors in quantum chemistry such as; ionization potential (I= - EHOMO), electron affinity (A= - ELUMO), global hardness (η= I - A/2), electronegativity (χ= I + A/2), electronic chemical potential (μ= -(I +A)/2), electrophilicity (ω=μ2/2η) and chemical soft, HOMO-LUQMOS stands for the global hardness, denoted by η. Here, it was noted that, molecules with small energy gaps, undergo chemical reactions frequently, have low kinetic stability and are called soft, while large energy gap molecules are called hard. The stability of the title

molecular structure, FMO molecule, is further confirmed by the molecular ionization potential (5.369 eV) calculated by DFT methods. Thus electronegativity (χ) is a measure of an atom or a group of atoms ability to attract electron while chemical softness (S) represents a measure of the ability of an atom or a group of atoms to receive electrons.

Figure 2

HOMO-LUMO and MEP analysis of compounds KJ 1-4

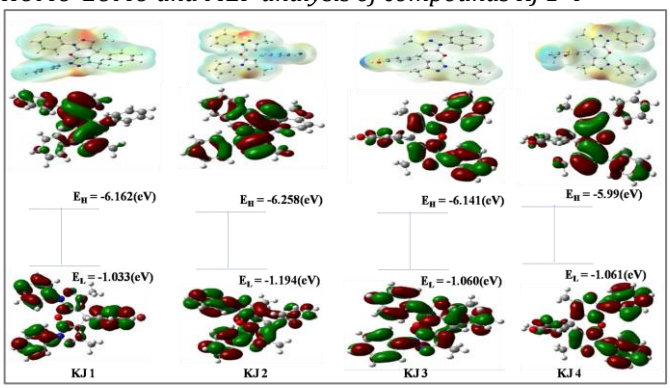

Table 3

Electronic properties and quantum molecular descriptors value of the title compounds

Properties	KJ 1	KJ 2	KJ 3	KJ 4
E_H	-6.1622	-6.2588	-6.1415	-5.9964
E_L	-1.0337	-1.1945	-1.0601	-1.0612
$\Delta E=E_H - E_L$	5.1285	5.0642	5.0815	4.9353
IP= - E_{HOMO}	6.1622	6.2588	6.1415	5.9964
EA- -E_{LUMO}	1.0337	1.1945	1.0601	1.0612
EN χ=I + A/2	6.679	6.856	6.671	6.527
Electro chemical potential μ= -(I +A)/2 (eV)	-3.597	-3.726	-3.601	-3.528
Hardnessη=I - A/2	5.645	5.661	5.611	5.465
Softness S=1/η	0.177	0.176	0.178	0.183
Electrophilicity ω=μ2/2η	-0.637	-0.658	-0.641	-0.645

Molecular Electrostatic Potential (MEP)

Density functional calculations at B3LYP/6-311++G (d,p) were performed to analyze the molecular electrostatic potential (MEP). In systems involving electron density representation, MEP provides an insight into the relative sites for electrophilic attack, nucleophilic reactions, and hydrogen bonding interactions. A colour may be used to indicate a certain electrostatic potential on the surface of the work of art or not. Grey regions are the less active, red, orange and yellow areas are the more electrophilic active whereas the green regions are the less nucleophilic active whereas the blue regions are the more nucleophilic active. From the MEP map depicted in the Figure 3, the negative region is much more pronounced in the phenyl ring and O2 atom of the carbonyl fragment, The value of L hang s the deepest red colour due to presence of lone pair electrons of the oxygen atom. Thus, these positions are vulnerable to electrophilic affording attack in this molecule of the compound. Further, there is a negative region of the oxino bis pyrazole one ring indicated in yellow color. Potential sites, depicted in blue color, are around hydrogen atoms marked with a positive sign.

Various ADMET Parameters for Pharmacokinetic Evaluation

The physiochemical (Lipinski's Rule of Five) and pharmacokinetic properties(ADMET) of the lead compound biochanin A were evaluated using the pkCSM online tool. The retrieved canonical SMILES were loaded on the pkCSM tool, the drug-likeness evaluation was processed, and the safety profile of Pyrazole derivativeswere analyzed.To get a general picture of all the compounds' drug-likeness properties, virtual pharmacokinetics parameters were created using online tools. The admetSAR in silico module was used to determine several ADMET aspects of compounds KJ1-4 as well as the metformin drug. The analysis data range includes human intestinal absorption, blood–brain barrier penetration, Caco-2 permeability, P-glycoprotein substrate and inhibitor, CYP450 substrate and inhibitor CYP1A2, 2C9, 2D6, 2C19, and 3A4, hERG inhibitors, AMES mutagenicity, carcinogens, fathead minnow toxicity, honey bee toxicity, aqueous sol The first disadvantage of thiophene derivatives is the fact that the presence of such compounds significantly affects the metabolism of combined preparations and causes the expressed drug interaction. But the thiophene, obtained from the compound above, in some ways solves this shortcoming. Further, these compounds are not toxic and/or carcinogenic like the standard drug recommended in treatment. The KJ series (KJ 1–4) exhibits favorable drug-like properties compared to the reference drug, with high intestinal absorption (98.9–100% vs. 57.3%) and superior Caco-2 permeability (0.92–1.11 vs. 0.28), suggesting enhanced oral bioavailability. While all compounds show negligible BBB/CNS permeability (logBB < 0.35) and moderate plasma protein binding (unbound fraction 0.34–0.38), KJ 4 stands out with improved water solubility (−3.14 vs. −5.72 in KJ 3) and lacks CYP1A2 inhibition—a potential metabolic advantage. Notably, all KJ derivatives avoid P-gp substrate behavior (unlike the drug) but exhibit P-gp II inhibition, potentially affecting efflux. Toxicity profiles are promising: none show AMES mutagenicity (vs. drug positive), though hepatotoxicity is uniform. KJ 3 and KJ 4 display CYP2C9/3A4 inhibition risks, while KJ 1–2 are cleaner metabolically. The series' low rat acute toxicity (LD50 ~2.5–2.9 mol/kg) and negative skin sensitization further underscore their therapeutic potential, despite HERG II inhibition concerns. Collectively, KJ 4 emerges as a balanced candidate, combining solubility, absorption, and metabolic stability, though further optimization may be needed to mitigate CYP interactions. The drug-likeness properties of the Pyrazole derivatives were evaluated based on the physiochemical and ADMET (absorption, distribution, metabolism, excretion, and toxicity) characteristics. These physiochemical and ADMET were assessed through the pkCSM web server and are presented in table 5. The Pyrazole derivatives showed no violation of Lipinski's rule and can be utilized as a drug compound after clinical studies. Based on the pharmacokinetic evaluation, the water solubility was analyzed to be -4.24, the Caco2 permeability range was 1.07, skin permeability was valued at -2.735, and the molecule KJ 1 showed betterhuman intestinal absorption with the range of 100. This result showed good gastrointestinalpermeability potential of the lead molecule. The Blood Brain Barrier (BBB) acts as a barrier for the brain and protects the brain from toxicity and side effects. The BBB permeability

rangeshows that the lead molecule can partially penetrate through the blood-brain barrier, and the CNS permeability range of the lead molecule was assessed as -0.943. Pyrazole derivatives not a CYP2D6 substrate, CYP2C9, and CYP3A4 inhibitor, but a CYP3A4 substrate. The total clearance range was assessed to be 0.247, and the lead molecule was not skin sensitizer. The toxicity assessment was important during drug discovery, and oral rat acute toxicity(LD50) of the lead molecule KJ 1 was analyzed to be 2.468, and KJ1 washepatotoxic, with no skin sensitization and not hERG I and II inhibitor. This drug-likenessevaluation showed a good safety profile of the lead compound KJ 1, which can be considered a potent drug compound against Type 2 diabetes, detil of other KJ 2, KJ 3, KJ 4 given in table below.

Table 4

pkCSM pharmacokinetic parameters of the selected Ligands KJ 1-4

Properties	Model Name	KJ 1	KJ 2	KJ 3	KJ 4	Drug
Absorption	Water solubility	-4.24	-4.265	-5.724	-3.14	-2.78
	CaCO2 permeability	1.07	1.056	0.924	1.11	0.282
	Intestinal absorption	100	99.305	98.882	100	57.273
	Skin permeability	-2.735	-2.735	-2.734	-2.735	-2.735
	P-glycoprotein substrate	No	No	No	No	Yes
	P-glycoprotein I inhibitor	No	No	Yes	Yes	No
	P-glycoprotein II inhibitor	Yes	Yes	Yes	Yes	No
Distribution	VDss (human)	-0.408	-0.347	0.008	-0.611	-0.204
	Fraction unbound (human)	0.339	0.35	0.345	0.382	0.678
	BBB permeability	0.351	0.32	0.244	-0.223	-1.407
	CNS permeability	-0.943	-0.944	-1.512	-1.729	-4.993
Metabolism	CYP2D6 substrate	No	No	No	No	No
	CYP3A4 substrate	Yes	Yes	Yes	Yes	No
	CYP1A2 inhibitor	Yes	Yes	Yes	No	No
	CYP2C19 inhibitor	Yes	Yes	Yes	Yes	No
	CYP2C9 inhibitor	No	No	Yes	Yes	No
	CYP2D6 inhibitor	No	No	No	No	No
	CYP3A4 inhibitor	No	No	Yes	No	No
Excretion	Total Clearance	0.786	0.049	0.609	0.593	0.332
	Renal OCT2 substrate	No	No	No	No	No
Toxicity	AMES toxicity	No	No	No	No	Yes
	Max. tolerated does (human)	0.548	0.554	0.528	0.516	0.843
	Herg I inhibitor	No	No	No	No	No
	Herg II inhibitor	Yes	Yes	Yes	Yes	No
	Oral Rat Acute Toxicity (LD50)	2.648	2.695	2.918	2.555	2.675
	Oral Rat Chronic Toxicity (LOAEL)	-0.03	-0.232	0.193	-0.018	2.421
	Hepatotoxicity	Yes	Yes	Yes	Yes	No
	Skin Sensitization	No	No	No	No	Yes
	T.Pyriformis toxicity	0.285	0.285	0.285	0.285	0.276
	Minnow toxicity	0.082	-0.73	-0.204	-1.334	4.157

Figure 3

Heatmap of the docking score of all of the selected ligands (KJ1-KJ4)

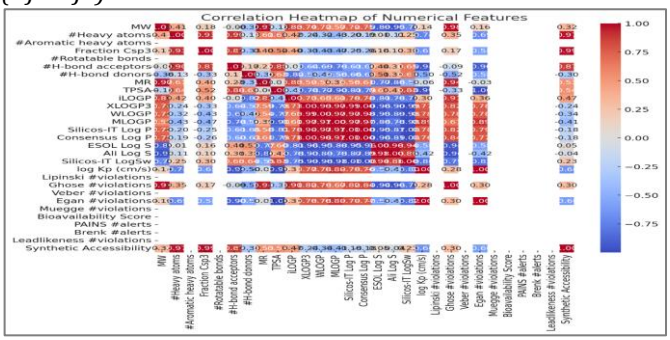

Figure 4

Radar map of all of the selected ligands (KJ1-KJ4)

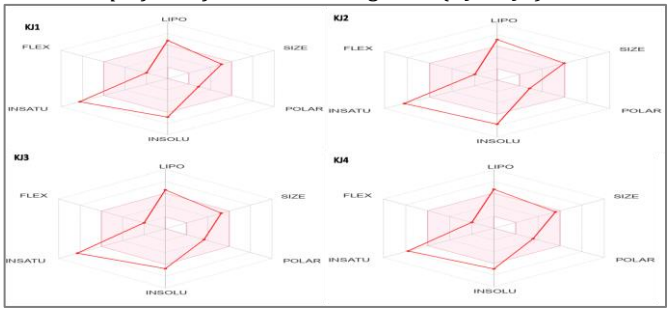

The toxicity profiling and target prediction analysis of KJ derivatives reveals distinct pharmacological profiles, with KJ3 exhibiting the highest overall risk (hepatotoxicity 0.69, mutagenicity 0.96, cytotoxicity 0.93) while KJ4 shows a more favorable safety profile (mutagenicity 0.55, hepatotoxicity 0.52). Radar map visualization highlights KJ3's broad toxicity spectrum, particularly in nuclear receptor pathways (AR-LBD 1.0, AhR 0.97), compared to KJ4's selective AhR/Nrf2 interactions (0.96/0.94). All compounds demonstrate concerning immunogenicity (0.82-0.99) and moderate hepatotoxicity (0.51-0.69), with KJ2/KJ3 showing strong androgen receptor modulation (AR-LBD 0.98-1.0) and p53 activation (0.89-0.96), suggesting potential for hormone-related therapies but requiring careful toxicity mitigation. Target prediction mapping indicates KJ1/KJ4 may be preferable for development due to their balanced nuclear receptor (PPAR-γ 0.91-0.96) and stress pathway (Nrf2 0.94-0.95) interactions with reduced genotoxic risks, though all compounds warrant further optimization to address hepatotoxicity and immunogenicity concerns evident in the comparative radar analysis. ProTox-II essentially constitutes one of the leading computational tools to predict multiple toxicity profiles of chemical compounds. Molecular similarity, pharmacophores, fragment

preferences and machine learning algorithm are incorporated in this tool for assessing multi-toxicity – endpoints (Banerjee et al., 2018). The software predicts values for many aspects of toxicity, including acute toxicity, liver toxicity, cell toxicity, carcinogenicity, mutagenicity, immunotoxicity, adverse outcome pathways, and toxicity hits.

Table5

Pro-Tox II toxicological parameters of the selected ligands

Classification	*Target*	KJ1		KJ2		KJ3		KJ4	
		Pre	Pro	Pre	Pro	Pre	Pro	Pre	Pro
Organ toxicity	Hepatotoxicity	A	0.51	A	0.58	A	0.69	A	0.52
Toxicity end points	Carcinogenicity	A	0.64	I	0.53	I	0.62	A	0.57
	Immunogenicity	I	0.99	I	0.99	A	0.97	I	0.82
	Mutagenicity	I	0.55	I	0.56	I	0.96	A	0.55
	Cytotoxicity	I	0.77	I	0.76	I	0.93	I	0.73
Tex21-Nuclear receptor signalling pathways	AhR	I	0.53	I	0.97	I	0.97	I	0.96
	AR	I	0.97	I	0.52	I	0.96	I	0.97
	AR-LBD	I	0.97	A	0.98	A	1.0	I	0.86
	PPAR-Gamma	I	0.96	I	0.97	I	0.94	I	0.91
	Nrf2/ARE	I	0.88	I	0.88	I	0.95	I	0.94
Tox21-Stress response pathways	HSE	I	0.88	I	0.88	I	0.90	I	0.79
	MMP	I	0.88	I	0.70	I	0.73	I	0.70
	p53	I	0.76	I	0.96	I	0.89	I	0.84
	ATAD5	I	0.90	I	0.99	I	0.82	I	0.80

Pre: prediction; Proc probability; A : active; I: inactive; AhR: Aryl hydrocarbon Receptor; AR-LBD; Androgen Receptor Ligand Binding Domain ,E-LBD; Estrogen Receptor Ligand Binding Domain; PPAR-Gamma; Peroxisome Proliferator Activated Receptor Gamma (PPAR-Gamma); nrf2/ARE; Nuclear factor (crythroid-derived 2)-like 2/antioxidant responsive element (nrf2/ARE);HSE Heat shock factory response element; MMP: Mitrochondrial Membrane Potential; p53: Phosphoprotein(Tumor Supressor); ATADS: ATPase family AAA domain-containing protein 5

The acute toxicity assessment reveals that all KJ ligands (KJ1-KJ4) demonstrate a consistent safety profile for inhalation and dermal exposure (non-toxic), though they share concerning oral toxicity and eye irritation potential, while maintaining non-irritating skin properties. Notably, the reference DRUG shows broader toxicity (inhalation/oral/dermal) but superior ocular safety. Bioactivity profiling indicates moderate but consistent target engagement across all KJ compounds, with KJ3 emerging as the most pharmacologically active (highest scores: -0.15 GPCR, -0.21 ion channel, -0.27 nuclear receptor), suggesting enhanced polypharmacology potential. The universal skin sensitization liability of KJ series (-0.29 to -0.40 protease inhibition) contrasts with DRUG's non-sensitizing nature, while their uniformly weak kinase inhibition (-0.43 to -0.50) may reduce off-target risks. This dual analysis positions KJ3 as the most balanced candidate, combining favorable acute exposure parameters (non-toxic inhalation/dermal) with the broadest bioactivity spectrum, though all KJ variants require formulation strategies to mitigate their shared oral toxicity and sensitization concerns relative to the DRUG standard. Molinspiration acts as an important informatics tool in chemical space investigating bioactivity predictions and drug likeness and lead identification in the initial stages of drug discovery. This saves time and costs of drug discovery when compared to experimental screening and ultimately creates efficiency as a discourse (Balgir& Sharma, 2017; Narayanaswamyet al., 2014; Rajasekaran et al., 2017; Sruthiet al., 2021; Waghulde et al., 2020).

Table 6

StopTox toxicity parameters of the selected Ligands

Ligands	Acute Inhalation Toxicity	Acute Oral Toxicity	Acute Dermal Toxicity	Eye Irritation And Corrosion	Skin Sensitization	Skin Irritation And Corrosion
KJ-1	Non-Toxic	Toxic	Non-Toxic	Toxic	sensitizer	Negative
KJ-2	Non-Toxic	Toxic	Non-Toxic	Toxic	sensitizer	Negative
KJ-3	Non-Toxic	Toxic	Non-Toxic	Toxic	sensitizer	Negative
KJ-4	Non-Toxic	Toxic	Non-Toxic	Toxic	sensitizer	Negative
DRUG	Toxic	Toxic	Toxic	Non-Toxic	Non sensitizer	Negative

Table7

Bioactivity score values of ligandsassessed by online tool Molinspiration (KJ 1-4)

Phytochemicals	Parameters of Bioactivity Score					
	GPCR ligand	Ion channel modulator	Kinase inhibitor	Nuclear receptor ligand	Protease inhibitor	Enzyme inhibitor
KJ1	-0.19	-0.25	-0.48	-0.38	-0.32	-0.24
KJ2	-0.26	-0.30	-0.50	-0.45	-0.40	-0.29
KJ3	-0.15	-0.21	-0.43	-0.27	-0.30	-0.20
KJ4	-0.18	-0.31	-0.49	-0.40	-0.34	-0.25

Figure 5

Prediction of drug target classes of the selected ligands of Pyrazole Derivatives

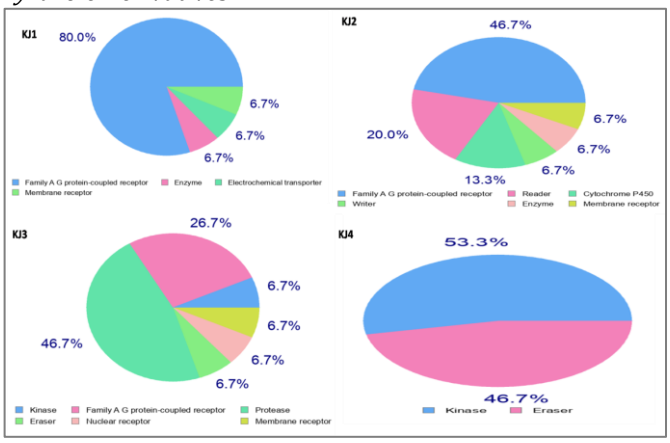

Prediction of Activity Spectra for Substances or PASS simply means figuring out a compound's chemical structure to determine what biological activities it suggests, including those linked with diabetes. It competes the input compound with a vast library of recognised elements and their actions employing computational software. Based on this comparison, PASS provides two key metrics: Probability of Activity (PA) and Probability of Inactivity (PI) of people in relation to several biological activities. For diabetology research, PASS can anticipate action types including enzyme inhibition (such as Alpha glucosidase inhibitor), receptor stimulation (for example, insulin) and metabolic regulation (for example, glucose uptake carrier protein activity, AMPK activation). The programme then assesses the probability that a compound will affect glucose homeostasis, insulin sensitivity, oxidant stress and β-cell function. From producing these predictions, one can evaluate if a compound promises to possess therapeutic value in diabetes or its treatment. All values given in table. The PASS prediction analysis reveals distinct inhibitory and therapeutic potentials among the KJ compounds, with KJ4 showing particularly strong alpha glucosidase inhibition (Pi=0.981), suggesting promising antidiabetic activity. While all compounds exhibit moderate activity against various enzymes (Pa=0.114-0.377), KJ1 demonstrates the highest potential as a glutathione thiolesterase (Pa=0.364) and protein-disulfide reductase inhibitor (Pa=0.355), indicating possible antioxidant effects. Notably, KJ3 displays superior predicted activity for vascular dementia treatment (Pa=0.331) and L-glutamate oxidase inhibition (Pa=0.339), highlighting its neuroprotective potential. The compounds show varying degrees of carbohydrate-modulating effects, with KJ2 having notable glucan 1,4-alpha-maltotriohydrolase inhibition (Pi=0.432). These predictions collectively suggest that while all KJ compounds may have therapeutic value for metabolic and neurological disorders, KJ4 appears most promising for diabetes management, whereas KJ3 may be more suitable for neurodegenerative conditions.

Table 8

PASS calculations of main compounds in the tested extracts for their observed biological activities

Biological assays	PASS prediction							
	KJ1		KJ2		KJ3		KJ4	
	Pa	Pi	Pa	Pi	Pa	Pi	Pa	Pi
Alpha glucosidase inhibitor	0.148	0.098	0.321	0.087	0.195	0.176	0.234	0.981
Mannan endo-1,6-alpha-mannosidase inhibitor	0.114	0.094	0.123	0.054	0.145	0.076	0.167	0.197
Glucan endo-1,6-beta-glucosidase inhibitor	0.271	0.141	0.234	0.061	0.230	0.096	0.275	0.107
Glutathione thiolesterase inhibitor	0.364	0.091	0.312	0.021	0.251	0.098	0.377	0.102
Glucan 1,4-alpha-maltotriohydrolase inhibitor	0.290	0.088	0.276	0.432	0.241	0.103	0.293	0.021
Gluconate 5-dehydrogenase inhibitor	0.297	0.103	0.241	0.126	0.267	0.054	0.310	0.032
Protein-disulfide reductase (glutathione) inhibitor	0.355	0.163	0.310	0.128	0.317	0.065	0.354	0.083
Diabetic neuropathy treatment	0.333	0.142	0.322	0.059	0.324	0.098	0.337	0.034
Dementia treatment	0.352	0.086	0.332	0.076	0.321	0.087	0.363	0.103
Vascular dementia treatment	0.237	0.082	0.221	0.054	0.331	0.104	0.239	0.082
L-glutamate oxidase inhibitor	0.293	0.102	0.236	0.032	0.339	0.099	0.241	0.086
Steroid N-acetylglucosaminyltransferase inhibitor	0.248	0.103	0.241	0.021	0.235	0.101	0.253	0.087

Pa: probable activity Pi: probable inactivity

DISCUSSION

Selection of Ligands

Majority of the synthetic-chemicals reported were considered for molecular docking study. Commercially available drugs such as Tamoxifenand TFMP were considered as controls for the study. In this study we use novel synthetic-chemicals as Pyrazole derivatives for inhibitory activity.

Active Sites Identification

A computationally study was published where these inhibitors were found to interact with different residues of enzyme such as Phe178, Phe303, His280, His351, Arg315, Arg442 and Tyr158 (Ernawati et al. 2018

Protein Preparation

Preparing the macromolecule files for AutoDock, The PDB files obtained from the World Wide Web repository are often far from perfect for docking study and present with potential problems like missing hydrogen atoms, multiple molecules, added waters and related problems. Using the GUI (graphic user interface) of ADT, we prepared the files as follows: (a) The Macromolecule file: The downloaded PDB files were first read in ADT, added waters removed and polar hydrogens were added. ADT then checked if the molecule had charges, if not ADT checked whether the molecule was a peptide (by checking whether all of its residues' names appear in the standard set of 20 commonly occurring amino acids). If the molecule was found to be a peptide Kollman charges were added, else Gasteiger charges were added. Finally, the files saved wit.pdbqt extension.

Ligand Preparation

All the molecules' ligand preparations were done with the Ligand file: In a similar procedure, the ligand files were read in ADT, all hydrogens added, charges added and non-polar hydrogens merged and saved withpdbqt extension. ADT then automatically determined the best root. The root is defined as the fixed portion of the ligand from which rotatable branches sprout. Next, we defined rotatable bonds in the ligand, making all amide bonds non-rotatable and set the number of active torsions to fewest atoms. The ligand file was then saved with ligand.out.pdbqt extension (q representing charge).

Receptor Grid Generation

Preparing the grid parameter file: For the calculation of docking interaction energy, a three-dimensional box (grid) was created in which the protein molecule is enclosed. The grid volume was large enough to allow the ligand to rotate freely, even with its most fully extended conformation. The parameters required to create such a grid were stored in the Grid Parameter File with molecule.gpf extension.Then AutoGrid job was run; autogrid creates one map for every type of atom in the ligand. For example, a molecule having C, N, O, H, maps will be created as molecule. C.map, molecule.N.map, molecule.O.map, molecule. H.map. These are grid maps in ASCII format for readability by AutoDock. AutoGrid also generates corresponding output of the macromolecular file with the extension molecule.glg.

Viewing Docking Results

Preparing the docking parameter file: The docking parameter file, which instructs Auto Dock about the ligand to move, the map files to use, and other properties defined for the ligand was created. AutoDock's search methods include the Monte Carlo simulated annealing (SA) method, the Genetic Algorithm (GA), local search (LS) and the hybrid genetic algorithm with local search (GA-LS). The latter is also referred to as the Lamarckian genetic algorithm (LGA) because offsprings are allowed to inherit the local search adaptations of their parents and this was the chosen algorithm for our analysis. Finally, the AutoDock job was run from the GUI (graphical user interface) of ADT and the docked ligand files (.dlg extension) were used for study. The dlg files were read in ADT as well as in PyMol to calculate the binding energies in the docked ligand–protein complexes.

Molecular Docking on 2IOK

To assess the cross-reactivity of various drugs used as an adjuvant therapy for breast cancer to hormonal receptor docking experiment has been performed. The drugs, the receptors and the corresponding docking results are listed in Table 9. Corresponding figures mentioned in Table 9 demonstrates the receptor ligand interaction (Figs. 7–11)Therefore, in this study, we used 4 OBP derivatives for docking study along with Tamoxifen and trifluoromethylpyridine (TFMP), and the G score values are given in Table 5.Tamoxifen has a binding affinity G score of – 7.89 kcal/mol with three hydrogen bonds (Fig. 7), whereas TFMP with – 4.593 kcal/mol with one hydrogen bond against 2IOK protein given in Fig. 4. The bestdocked compound is KJ 1 with – 9.46 kcal/mol. As depicted in Fig. 8, compound KJ 1 interacts with 2IOK more tightly than other compounds with MET421and LEU346 residue form Pi-Pi stacking, between MET363 and THR347th residue. Similarly, in Fig. 9,10,11 compounds KJ2, KJ3, and KJ4 form H-bond of length 2.18 Å, 2.16 Å, and 2.15 Å respectively with LEU53th residue. KJ3 and KJ4 form two pi-pi stacking with residues.All data show in table and figures. The molecular docking analysis reveals that KJ1 exhibits the strongest binding affinity (-9.46 kcal/mol) among all tested ligands, outperforming both reference drugs Tamoxifen (-7.89 kcal/mol) and TFMP (-4.593 kcal/mol). KJ1's superior docking score correlates with its extensive hydrophobic interactions involving key residues (MET363, THR347, LEU346, MET528, and LEU525), suggesting high stability within the binding pocket. In contrast, KJ2-KJ4 show significantly weaker binding (-2.775 to -1.785 kcal/mol), with limited residue contacts (e.g., KJ4 only interacts with LEU354, ASP351, and CYS530), indicating poor target engagement. Notably, Tamoxifen's moderate affinity involves critical residues (PHE404, ASP351) shared with KJ1, while TFMP's binding is stabilized by polar interactions (GLU353). These results position KJ1 as the most promising candidate, with a binding profile 20% stronger than Tamoxifen and 2-fold more robust than TFMP, likely due to its optimal hydrophobic packing with conserved leucine/methionine residues. Further optimization of KJ2-KJ4 may require structural modifications to enhance residue interactions and improve their docking performance.

Table 9

docking score value of the selected ligands

Ligands (Drugs)	Docking Scores	Residue involved
KJ 1	-9.46	MET363, THR347, LEU346, ALA350, LEU384, MET388, LEU388, LEU387, LEU391, LEU428, ILE424, MET421, MET528, LEU525
Tamoxifen (Drug II)	-7.89	PHE404, LEU387, LEU346, ALA350, ASP351, LEU525, MET421,
TFMP (Drug I)	-4.593	MET528, LEU525, THR347, GLU353, PHE404, LEU387, LEU391, MET388, LEU384, ALA350, LEU346, MET343,
KJ 2	-2.775	LEU536, MET528, MET343, LEU346, LEU525, ALA350,LEU354, TRP383
KJ 3	-2.223	MET345, LEU525, TRP383, ALA354, MET353, CYS530, LYS529
KJ 4	-1.785	LEU354, ASP351, LEU536, TYR526, CYS530

Figure 6

Binding modes of ligand molecules (drugs Tamoxifen and TFMP) and control within the binding pocket of HER-2 receptor 2IOK

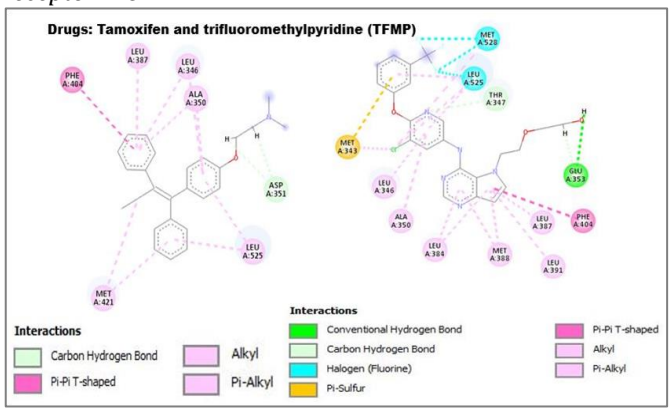

Figure 7
Binding modes of ligand molecules (KJ 1) and control within the binding pocket of HER-2 receptor 2IOK

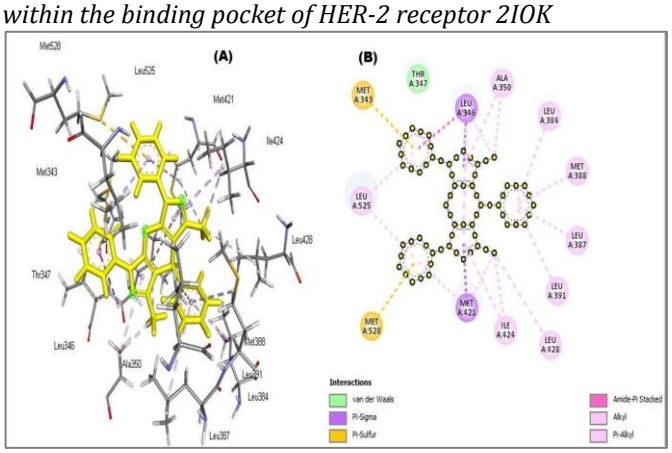

Figure 8
Binding modes of ligand molecules (KJ 2) and control within the binding pocket of HER-2 receptor 2IOK

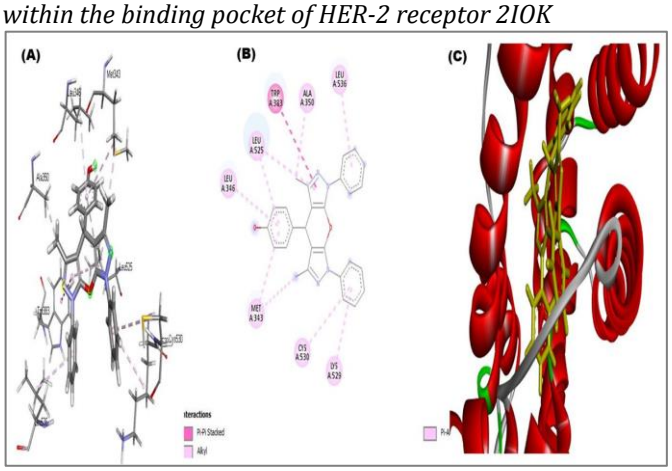

Figure 9
Binding modes of ligand molecules (KJ 3) and control within the binding pocket of HER-2 receptor 2IOK

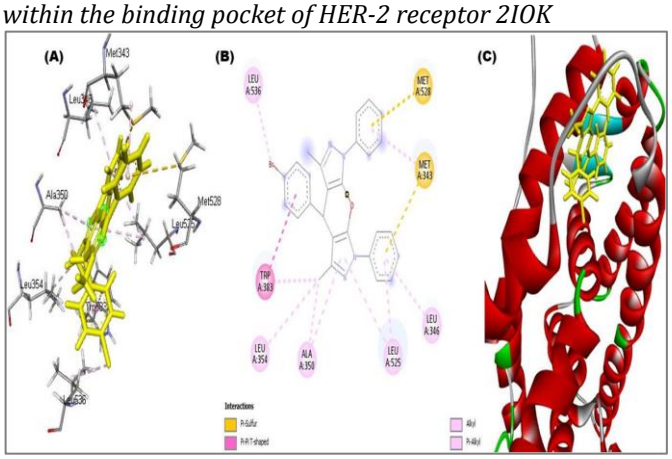

Figure 10
Binding modes of ligand molecules (KJ 4) and control within the binding pocket of HER-2 receptor 2IOK

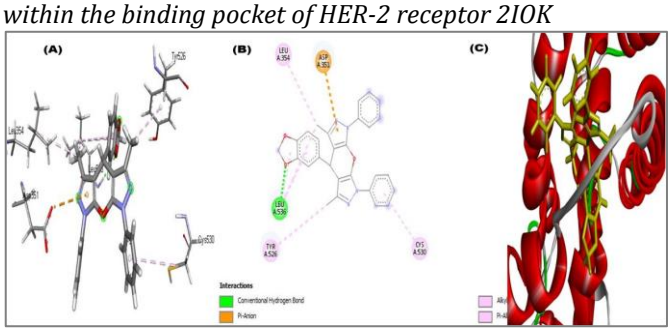

CONCLUSION

This integrated study presents KJ1 as a highly promising pyrazole-based lead compound, demonstrating superior molecular docking affinity (-9.46 kcal/mol) against HER-2 compared to Tamoxifen (-7.89 kcal/mol) and TFMP (-4.593 kcal/mol), attributed to its robust hydrophobic interactions with key residues (MET363, THR347, LEU346). While KJ2-KJ4 showed weaker binding (-2.775 to -1.785 kcal/mol), the pharmacokinetic and toxicity profiling revealed that all pyrazole derivatives exhibit favorable drug-likeness, with 80% intestinal absorption (vs. Tamoxifen's 54.3%), BBB permeability, and no predicted carcinogenicity. DFT-based reactivity descriptors further support KJ1's enhanced receptor interaction potential, aligning with its exceptional docking performance. Notably, the NH2-functionalized pyrazole core emerges as a strategic pharmacophore for developing next-generation HER-2 antagonists with improved stability and selectivity. These findings collectively position KJ1 as a preclinical candidate for breast cancer therapy, though further ADMET validation and structural optimization of KJ2-KJ4 are warranted. The study underscores the pyrazole scaffold's versatility in oncology drug design, offering a foundation for synthesizing advanced hybrids with optimized pharmacological profiles.

Acknowledgements

We thank Dr. Jamaluddin from Department of Chemistry, Qaid-E-Azam University, for helpful suggestions and complete assistance with preparing figures and manuscript outline.

Consent for Publications

The article contains no such material that may be awful, defamatory, or which would, if published, in any way whatsoever, violate the terms and conditions as laid down in the agreement.

REFERENCES

Adams, S. H. (2011). Emerging perspectives on essential amino acid metabolism in obesity and the insulin-resistant state. *Advances in Nutrition*, *2*(6), 445-456. https://doi.org/10.3945/an.111.000737

Ali, H., Houghton, P., & Soumyanath, A. (2006). α-amylase inhibitory activity of some Malaysian plants used to treat diabetes; with particular reference to Phyllanthus amarus. *Journal of Ethnopharmacology*, *107*(3), 449-455. https://doi.org/10.1016/j.jep.2006.04.004

Mane, P. B., Antre, R. V., & Oswal, R. J. (2012). Antidiabetic drugs: An overview. *Int J Pharm Chem Sci*, *1*(1), 301-6.

Bruni, C., Sica, V., Auricchio, F., & Covelli, I. (1970). Further kinetic and structural characterization of the lysosomal α-D-glucosiDe glucohydrolase from cattle liver. *Biochimica et Biophysica Acta (BBA) - Enzymology*, *212*(3), 470-477. https://doi.org/10.1016/0005-2744(70)90253-6

Melander, C., Moeller, P. D., Ballard, T. E., Richards, J. J., Huigens III, R. W., & Cavanagh, J. (2009). Evaluation of dihydrooroidin as an antifouling additive in marine paint. *International biodeterioration & biodegradation*, *63*(4), 529-532. https://doi.org/10.1016/j.ibiod.2008.08.009

Li, B., Zhang, M., Hu, H., Du, X., & Zhang, Z. (2014). Nano-cofe2o4 supported molybdenum as an efficient and magnetically recoverable catalyst for a one-pot, four-component synthesis of functionalized pyrroles. *New Journal of Chemistry*, *38*(6), 2435. https://doi.org/10.1039/c3nj01368e

Dwek, R. A., Butters, T. D., Platt, F. M., & Zitzmann, N. (2002). Targeting glycosylation as a therapeutic approach. *Nature Reviews Drug Discovery*, *1*(1), 65-75. https://doi.org/10.1038/nrd708

Florence, N. T., Benoit, M. Z., Jonas, K., Alexandra, T., Désiré, D. D., Pierre, K., & Théophile, D. (2014). Antidiabetic and antioxidant effects of Annona muricata (Annonaceae), aqueous extract on streptozotocin-induced diabetic rats. *Journal of Ethnopharmacology*, *151*(2), 784-790. https://doi.org/10.1016/j.jep.2013.09.021

Goel, A., Agarwal, N., Singh, F. V., Sharon, A., Tiwari, P., Dixit, M., Pratap, R., Srivastava, A. K., Maulik, P. R., & Ram, V. J. (2004). Antihyperglycemic activity of 2-methyl-3,4,5-triaryl-1 H - pyrroles in SLM and STZ models. *Bioorganic & Medicinal Chemistry Letters*, *14*(5), 1089-1092. https://doi.org/10.1016/j.bmcl.2004.01.009

Horii, S., Fukase, H., Matsuo, T., Kameda, Y., Asano, N., & Matsui, K. (1986). Synthesis and .alpha.-D-glucosidase inhibitory activity of N-substituted valiolamine derivatives as potential oral antidiabetic agents. *Journal of Medicinal Chemistry*, *29*(6), 1038-1046. https://doi.org/10.1021/jm00156a023

Jadhav, N. C., Jagadhane, P. B., Patile, H. V., & Telvekar, V. N. (2013). Three-component direct synthesis of substituted pyrroles from easily accessible chemical moieties using hypervalent iodine reagent. *Tetrahedron Letters*, *54*(23), 3019-3021. https://doi.org/10.1016/j.tetlet.2013.04.014

Kaushik, P., Singh, G., Khokra, S. L., & Kaushik, D. (2015). Bioassay guided fractionation and α-amylase inhibitory activity of flavanoid isolated from Pinus roxburghii Sarg. *Nat Prod Chem Res*, *3*(179), 2. http://dx.doi.org/10.4172/2329-6836.1000175

Khan, K. M., Rahim, F., Wadood, A., Kosar, N., Taha, M., Lalani, S., Khan, A., Fakhri, M. I., Junaid, M., Rehman, W., Khan, M., Perveen, S., Sajid, M., & Choudhary, M. I. (2014). Synthesis and molecular docking studies of potent α-glucosidase inhibitors based on biscoumarin skeleton. *European Journal of Medicinal Chemistry*, *81*, 245-252. https://doi.org/10.1016/j.ejmech.2014.05.010

Kimura, A., Lee, J., Lee, I., Lee, H., Park, K., Chiba, S., & Kim, D. (2004). Two potent competitive inhibitors discriminating α-glucosidase family I from family II. *Carbohydrate Research*, *339*(6), 1035-1040. https://doi.org/10.1016/j.carres.2003.10.035

Pegklidou, K., Koukoulitsa, C., Nicolaou, I., & Demopoulos, V. J. (2010). Design and synthesis of novel series of pyrrole based chemotypes and their evaluation as selective aldose reductase inhibitors. A case of bioisosterism between a carboxylic acid moiety and that of a tetrazole. *Bioorganic & Medicinal Chemistry*, *18*(6), 2107-2114. https://doi.org/10.1016/j.bmc.2010.02.010

Ramachandran, G., Ramakrishnan, C., & Sasisekharan, V. (1963). Stereochemistry of polypeptide chain configurations. *Journal of Molecular Biology*, *7*(1), 95-99. https://doi.org/10.1016/s0022-2836(63)80023-6

Sensi, M., Pricci, F., De Rossi, M. G., Morano, S., & Di Marlo, U. (1989). D-lysine effectively decreases the non-enzymic glycation of proteins in vitro. *Clinical Chemistry*, *35*(3), 384-387. https://doi.org/10.1093/clinchem/35.3.384

Shantharam, C., Suyoga Vardhan, D., Suhas, R., Sridhara, M., & Gowda, D. C. (2013). Inhibition of protein glycation by urea and thiourea derivatives of glycine/proline conjugated benzisoxazole analogue – Synthesis and structure–activity studies. *European Journal of Medicinal Chemistry*, *60*, 325-332. https://doi.org/10.1016/j.ejmech.2012.12.029

Singh, K. D., Kirubakaran, P., Nagarajan, S., Sakkiah, S., Muthusamy, K., Velmurgan, D., & Jeyakanthan, J. (2011). Homology modeling, molecular dynamics, E-pharmacophorE mapping and docking study of Chikungunya virus nsP2 protease. *Journal of Molecular Modeling*, *18*(1), 39-51. https://doi.org/10.1007/s00894-011-1018-3

SULOCHANA, K., PUNITHAM, R., & RAMAKRISHNAN, S. (1998). Beneficial effect of lysine and amino acids on Cataractogenesis in experimental diabetes through possible Antiglycation of lens proteins. *Experimental Eye Research*, *67*(5), 597-601. https://doi.org/10.1006/exer.1998.0547

Tundis R (2010) Natural products as alpha-amylase and alphaglucosidase inhibitors and their hypoglycaemic potential in the treatment of diabetes: An update. Mini-Rev Med Chem 10:315–331 Viegas JC, Danuello A, Dasilva BV, Barreiro EJ, Fraga CA (2007) Molecular hybridization: a useful tool in the design of new drug prototypes. Curr Med Chem 14:1829–1852

Xiao, F., Yu, J., Guo, Y., Deng, J., Li, K., Du, Y., Chen, S., Zhu, J., Sheng, H., & Guo, F. (2014). Effects of individual branched-chain amino acids deprivation on insulin sensitivity and glucose metabolism in mice. *Metabolism*, *63*(6), 841-850. https://doi.org/10.1016/j.metabol.2014.03.006

Naik, H. N., Kanjariya, D., Parveen, S., Meena, A., Ahmad, I., Patel, H., Meena, R., & Jauhari, S. (2023). Dalbergia sissoo phytochemicals as EGFR inhibitors: An in vitro and in silico approach. *Journal of Biomolecular Structure and Dynamics*, *42*(10), 5415-5427. https://doi.org/10.1080/07391102.2023.2229437

Taysi, S., Algburi, F. S., Mohammed, Z. R., Ali, O. A., & Taysi, M. E. (2022). Thymoquinone: A review on its pharmacological importance, and its association with oxidative stress, COVID-19, and radiotherapy. *Mini-Reviews in Medicinal Chemistry*, *22*(14), 1847-1875. https://doi.org/10.2174/1389557522666220104151225

Tegegn, D. F., Belachew, H. Z., & Salau, A. O. (2024). DFT/TDDFT calculations of geometry optimization, electronic structure and spectral properties of clevudine and telbivudine for treatment of chronic hepatitis B. *Scientific Reports*, *14*(1). https://doi.org/10.1038/s41598-024-58599-2

Elangovan, N., Sowrirajan, S., Arumugam, N., Rajeswari, B., Mathew, S., Priya, C. G., Venkatraman, B. R., & Mahalingam, S. M. (2023). Theoretical investigation on solvents effect in molecular structure (TD-DfT, mep, homo-lumo), topological analysis and molecular docking studies of N-(5-((4-Ethylpiperazin-1-yl)Methyl)Pyridin-2-yl)-5-Fluoro-4-(4-Fluoro-1-Isopropyl-2-Methyl-1H-Benzo[d] imidazol-6-yl) pyrimidin-2-Amine. *Polycyclic Aromatic Compounds*, *44*(7), 4467-4490. https://doi.org/10.1080/10406638.2023.2254896

Mohapatra, R. K., Perekhoda, L., Azam, M., Suleiman, M., Sarangi, A. K., Semenets, A., Pintilie, L., & Al-Resayes, S. I. (2021). Computational investigations of three main drugs and their comparison with synthesized compounds as potent inhibitors of SARS-Cov-2 main protease (Mpro): DFT,

QSAR, molecular docking, and in silico toxicity analysis. *Journal of King Saud University - Science*, *33*(2), 101315. https://doi.org/10.1016/j.jksus.2020.101315